 doi:10.20944/preprints202009.0616.v1

Interfacial Crystallization within Liquid Marbles

Pritam Kumar Roy[a], Irina Legchenkova[a], Shraga Shoval[b], Edward Bormashenko[a,*]

[a]*Chemical Engineering Department, Engineering Faculty, Ariel University, P.O.B. 3, 407000, Ariel, Israel*
[b]*Industrial Engineering and Management Department, Engineering Faculty, Ariel University, P.O.B. 3, 40700, Ariel, Israel*
*Corresponding author: edward@ariel.ac.il

Abstract: We report interfacial crystallization in droplets of saline solutions placed on superhydrophobic surfaces and liquid marbles filled with the saline. Evaporation of saline droplets deposited on superhydrophobic surface resulted in the formation of cup-shaped millimeter-scaled residues. The formation of the cup-like deposit is reasonably explained within the framework of the theory of the coffee-stain effect, namely, the rate of heterogeneous crystallization along the contact line of the droplet is many times higher than in the droplet bulk. Crystallization within evaporated saline marbles, coated with lycopodium particles, depends strongly on the evaporation rate. Rapidly evaporated saline marbles yielded dented shells built of a mixture of colloidal particles and NaCl crystals. We relate the formation of these shells to the interfacial crystallization promoted by hydrophobic particles coating the marbles, accompanied with the upward convection flows supplying the saline to the particles, serving as the centers of interfacial crystallization. Convective flows prevail over the diffusion mass transport for the saline marbles heated from below.
Keywords: interfacial crystallization; liquid marble, hydrophobic particle; superhydrophobic surface; coffee-stain effect.

1. Introduction

Interfacial crystallization has attracted much interest of scientists in the field of condensed matter in the past decades [1-6]. Interfacial crystallization enables intelligent control of the morphology of crystals, nucleated in the vicinity of solid/liquid [1-3] or liquid/liquid interfaces [4-6], and some unique crystalline structures have been obtained, including nano-whiskers [4] and hybrid shish–kebab and shish–calabash structures [1-2]. Interfacial crystallization allowed manufacturing of energetic nano-crystals [3] and porous particles [5]. The complicated physico-chemical mechanisms of the interfacial crystallization were addressed in Refs. 7-10. We demonstrate in our communication that evaporated liquid marbles may be used for the interface-driven crystallization.

Liquid marbles, introduced in the pioneering investigations of Quéré *et al*., are non-stick droplets coated with nano- or micron-sized particles, which are usually hydrophobic [11-15]. Liquid marbles are not hermetically coated by the solid particles. The respirability of liquid marbles makes them suitable for the cultivation of microorganisms and cells [16-20]. Liquid marbles may also be used as mini-reactors and bio-reactors [21-22]. Kinetics of the evaporation of

Preprints (www.preprints.org) | NOT PEER-REVIEWED | Posted: 25 September 2020 doi:10.20944/preprints202009.0616.v1

liquid marbles was addressed in Refs. 23-26. Use of liquid marbles for non-traditional computing was reported recently [27-30]. Liquid marbles may be actuated by UV and IR light and Marangoni flows [31-33], and demonstrate obvious potential for micro-fluidics applications [34-35]. Actually, liquid marbles opened new horizons for the researches studying the liquid state of the matter. We report here the use of liquid marbles for the controlled interfacial crystallization.

2. Results

We carried out comparative experiments in which droplets of aqueous NaCl solutions were evaporated under conditions of superhydrophobicity when: i) naked aqueous NaCl solution droplets were evaporated when placed on superhydrophobic surfaces; ii) marbles filled with aqueous NaCl solution and coated with lycopodium powder (a strongly hydrophobic yellow-tan dust-like powder, consisting of the dry spores of clubmoss plants) were evaporated when placed on superhydrophobic substrates as depicted in **Figure 1**.

When naked saline droplets are evaporated on superhydrophobic surfaces, very different scenarios of evaporation are possible, namely the evaporation may take place under the pinned triple line, and under the sliding triple line as discussed in Ref. 36. The evaporation may be accompanied by the Cassie-Wenzel wetting transition and may take place within the Cassie wetting regime [36-37]. We studied evaporation of the naked saline droplets under ambient conditions (t=25°C) and also under the constant temperature of the substrate of t=70°C. The characteristic time scales of evaporation were $\tau_{ev} \cong 24\ min$ for the "slow" and $\tau_{ev} \cong 4\ min$ for the rapid evaporation processes.

Both of temperature regimes supplied very similar results, namely evaporation occurred under the slight variation in the apparent contact angle, i.e. $142° < \theta_{app} < 149°$, as shown in **Figure 2**, whereas the contact line was strongly pinned as demonstrated in **Movie S1** and **Movie S2**. Thus, it is reasonable to suggest that the evaporation took place within the Cassie wetting regime. The wetting regime at which high apparent contact angles are accompanied with the pronounced pinning of the triple line is inherent for the so-called "rose petal effect" [37-40]. However, in our experiments, the situation was much more complicated due to the crystallization of NaCl occurring in a course of evaporation of the droplets; and it is reasonable to suggest that high pinning of the triple line arises from the high affinity of water to NaCl crystals, formed in the vicinity of the triple line, as will be demonstrated in detail below.

3. Discussion

Evaporation resulted in the formation of the cup-shaped millimeter-scaled residues, shown in **Figs**. **1(a)-3(a**) and **Movies S1** and **S2**, and was observed for both slow and rapid evaporation regimes. It seems that the formation of this cup-like deposit may be explained within the framework of the theory of the coffee-stain effect developed in Refs. 41-42. The authors of Refs. 41-42 related the formation of coffee-stain deposits to a couple of main physical reasons, namely: contact line pinning and intensive evaporation from the edge of the drop. When the apparent contact angle is obtuse, we have one more geometric factor strengthening the evaporation rate in

Preprints (www.preprints.org) | NOT PEER-REVIEWED | Posted: 25 September 2020 doi:10.20944/preprints202009.0616.v1

the vicinity of the triple line, which is shown schematically in **Figure 4**. Consider two molecules evaporated from the sites labeled "I" and "II" depicted in **Figure 4**. A molecule evaporated from the site labeled "I" has a chance to be absorbed by a droplet, whereas a molecule evaporated from site "II" has a chance to be absorbed by the superhydrophobic substrate. This factor strengthens the evaporation rate in the vicinity of the triple line. A pinned contact line, in turn, induces an outward, radial fluid flow when there is evaporation at the edge of the drop; this flow replenishes the liquid that is removed from the edge and gives rise to the formation of the coffee-stain cup-like deposits shown **Figs**. **1(a)-3(a)** and discussed in detail in Refs. 41-42. Crystallization of NaCl at the circumference of the contact area, in turn, strengthens the effect of pinning. Thus, crystallization works as a positive feedback, enhancing the coffee-stain effect and providing the stability of the apparent contact angle in a course of evaporation, illustrated in **Figure 1a**. Our observations support recent experimental findings reported in Ref. 43, in which the crystallization of $CaCl_2$ salt in a droplet was investigated, and it was revealed that the crystallization rate along the contact line of the droplet is many times higher than in the direction of the droplet radius. Obviously, the heterogeneous crystallization prevails on the homogeneous bulk nucleation.

Now, consider the evaporation of liquid marbles filled with the NaCl solutions. In contrast to the naked saline droplets, the apparent contact angle of the marbles decreased gradually in a course of evaporation from *ca*. 150° to *ca*. 115°, as shown in **Figure 5** and **Movie S3**. It should be mentioned that the apparent contact angle of a liquid marble is not a "true interfacial angle", due to the fact that it is formed by the micro-rough surface of a marble coated with colloidal particles.

We establish that the eventual shape of the solid residue, built of the mixture of colloidal particles and NaCl crystals, depends strongly on the temperature of evaporation and the concentration of the solution. When the marble was slowly evaporated under ambient conditions, (the characteristic time of the process was $\tau_{ev} \cong 35\,min$) the process yielded a single relatively large (*ca*. 1 mm) NaCl crystal formed at the bottom of the evaporated saline marble.

The situation was rather different for rapidly evaporated liquid marbles. When evaporation was conducted under high temperatures (t=70°C), the characteristic time of the process was $\tau_{ev} \cong$ 5 min and two different scenarios of crystallization were observed. When the NaCl solutions were unsaturated (14.9% w/w and 8.1% w/w) the crystallization took place mainly at the base of the marble, yielding the flat residues shown in **Figure 6**. The most interesting and intriguing result was obtained under the rapid ($t = 70°C, \tau_{ev} \cong 5$ min) evaporation of saturated NaCl solutions. In this case, small crystals of NaCl (the characteristic size of crystals was *ca*. 10-50 μm) grew uniformly over the entire marble shell. In other words, the interface crystallization stimulated by the particles coating a marble took place [1-6]. The NaCl crystals merged with the colloidal particles, thus forming the uniform hemisphere-like dented shells depicted in **Figure 7(b) and Figure 8d**. The SEM images of the shells, representing the mixture of NaCl crystals and colloidal particles, are depicted in the inset **(c)** of **Figure 7.** The residues depicted in **Figures 7(b)** and **Figure 8d** are markedly stronger than the residues emerging at room temperature. It should be emphasized that in this case, the interfacial crystallization promoted by the hydrophobic particles

Preprints (www.preprints.org) | NOT PEER-REVIEWED | Posted: 25 September 2020 doi:10.20944/preprints202009.0616.v1

coating the marble was observed. The mass transport promoting the interfacial crystallization under slow and rapid evaporation is depicted schematically in **Figures 8a**, **c**.

The upward flow, supplying NaCl to the hydrophobic particles coating the marble, is reasonably attributed to the thermal convection, inevitable when a marble is placed on a hot plate. Consider that the change of the temperature of the saline in the course of evaporation was registered with the thermal camera as *ca*. $\Delta t \cong 25°$. In order to attain a qualitative understanding of the process occurring within the marbles under their evaporation, let us understand the hierarchy of time scales involved in the process. The characteristic time scale of evaporation is $\tau_{ev} \cong 5$ min. The characteristic time scale of the diffusion mass transport within the marbles/saline droplets is supplied by Eq. 1:

$$\tau_{diff} \cong \frac{(2R)^2}{D}, \quad (1)$$

where R is the radius of a marble and D is the diffusion coefficient of NaCl in water; substitution of $R \cong 1.0 \times 10^{-3}$m and $D \cong 1.5 \times 10^{-9} \frac{\mathrm{m}^2}{\mathrm{s}}$ yields the estimation $\tau_{diff} \cong 2.7 \times 10^3$s $\cong$ 45.0 min.

The characteristic time scale of thermal equilibration in the marbles heated from below τ_{eq} may be estimated as:

$$\tau_{therm} \cong \frac{(2R)^2}{\alpha}, \quad (2)$$

where $\alpha \cong 0.14 \times 10^{-6} \frac{\mathrm{m}^2}{\mathrm{s}}$ is the thermal diffusivity of saline (see Ref. 44); calculation with Eq. 2 yields the estimation $\tau_{therm} \cong 0.5$ min. Thus, the hierarchy of time scales supplied by Eq. 3 takes place:

$$\tau_{diff} \gg \tau_{ev} \gg \tau_{therm}\,. \quad (3)$$

We recognize from Eq. 3, that the diffusion mass transport is a slow process on the time scales of evaporation and thermal equilibration, occurring in the saline marbles subject to heating. Therefore, it is reasonable to attribute the dramatic influence exerted by temperature on the morphology of the eventual residue to the upward convective flows (shown schematically in **Figure 8c**) which supply saline to the hydrophobic particles, coating the marble and promoting the interfacial crystallization, and yielding entire shells shown in **Figure 7b**. Contrastingly, slow evaporation of the liquid marbles yielded flat deposits, shown in **Figure 8b,** containing the large (~1 mm) NaCl crystal formed at the base of the marble. This conclusion is supported by the direct calculation of the Peclet number, supplied by Eq. 4:

$$Pe = \frac{2Ru}{D}, \quad (4)$$

where u is the characteristic velocity of the convective flows (see **Figure 8c**). Direct visualization of the convective flows taking place within the heated marbles under $t = 70°C$ supplied the value of the typical velocity of convective flows estimated as $u \cong 0.3 \frac{\mathrm{mm}}{\mathrm{s}}$ (see **Movie S2**).

Substitution of the aforementioned values of the physical parameters yields the estimation: $Pe \cong 4 \times 10^2 \gg 1$. This means that within the regime of rapid evaporation of the saline marbles

Preprints (www.preprints.org) | NOT PEER-REVIEWED | Posted: 25 September 2020 doi:10.20944/preprints202009.0616.v1

the bulk convective flows prevail over the diffusion mass transport, thus justifying the suggested mechanism of shells' formation.

Our observations are in accordance with those reported in Ref. 45, in which crystallization during evaporation of saturated Na_2SO_4 and NaCl droplets was studied. The authors of Ref. 45 reported that on a hydrophobic surface, contrary to what happens for the hydrophilic one, the NaCl crystallization appears not at the liquid-air interface but rather at the solid-liquid interface. In our experiments, this was the case for both naked NaCl droplets evaporated on superhydrophobic surfaces and also for NaCl liquid marbles. Let us quote Ref. 45: "Sodium chloride crystals are found to form preferentially in contact with a nonpolar area (air or hydrophobic solid). This is an important observation, as hydrophobic treatments have been used frequently in the past to prevent crystallization and damage on buildings. Our observations suggest that this may be counterproductive due to the tendency of NaCl to crystallize on nonpolar surfaces". Our results support this conclusion; indeed, the sodium chloride crystals prefer to grow on hydrophobic surfaces in contact with NaCl solutions, filling naked droplets placed on superhydrophobic surfaces and saline marbles.

The dented shape of the shell emerging from the evaporation of saline marbles, shown in **Figures 8c-d,** is noteworthy. This shape resembles the shape of Leidenfrost droplets deposited on hot plates, discussed in Ref. 46. It is reasonable to attribute the formation of the dent to a gas pocket, formed by the evaporation of water when a marble is heated from below.

4. Conclusions

We conclude that the saline droplets placed on superhydrophobic surfaces and liquid marbles filled with saline demonstrate interfacial crystallization over the course of water evaporation. Evaporation of naked saline droplets resulted in the formation of cup-shaped millimeter-scaled residues. The formation of the cup-like deposit is reasonably explained within the framework of the theory of the coffee-stain effect [41-42]. Evaporated saline marbles heated from below gave rise to dented shells built of a mixture of colloidal particles and NaCl crystals. Qualitative analysis of the processes taking place under the evaporation of saline marbles support the assumption that the diffusion mass transport is a slow process on the time scales of evaporation and thermal equilibration of heated marbles. Formation of the entire shells built of the lycopodium and NaCl crystals under rapid evaporation of the heated saline marbles takes place under the high values of the Peclet numbers. We relate the formation of these shells to the interfacial crystallization promoted by the hydrophobic particles coating the marbles, accompanied by the upward convection flows supplying the saline to the hydrophobic particles.

5. Materials and Methods

The following materials were used in order to prepare the liquid marbles: deionized water (DI) from Millipore SAS (France) (specific resistivity $\hat{\rho} = 18.2\ \mathrm{M\Omega \cdot cm}$ at 25ºC, surface tension $\gamma =$ 72.9 mN/m; viscosity $\eta = 8.9 \times 10^{-4}\mathrm{Pa \cdot s}$) was used in the experiments. Sodium chloride (NaCl) was supplied by Melach Haaretz Ltd., Israel. Lycopodium powder (average diameter 50 μm) supplied by Fluka.

 doi:10.20944/preprints202009.0616.v1

Liquid marbles containing aqueous solution of NaCl were coated by lycopodium powder. 5-20 µL drops containing three different concentrations of aqueous NaCl solution (25.9% w/w; 14.9% w/w and 8.1% w/w) were used to prepare the liquid marbles. Saline droplets were deposited using a precise micro syringe on the superhydrophobic surface. The superhydrophobic surface covered with a layer of aforementioned powders. Rolling of droplets yielded the formation of marbles enwrapped with the specified hydrophobic powders and containing the solution.

Evaporation of liquid marbles and naked saline droplets was performed on a superhydrophobic surface. The evaporation process, carried out on the superhydrophobic surface, was studied at ambient conditions ($t = 25°C$) and 70°C, where 70°C was the temperature of the hot plate. The relative humidity was RH = 44%.

A Nikon 1 v3 camera, digital microscope BW1008-500X and filed emission scanning electron microscope (MAIA3 TESCAN) were used to capture images and movies of the marbles during evaporation. A Rame-Hart 500 goniometer was used to capture the side view of the liquid marbles during evaporation. Temperature distribution was studied using a Therm-App Pro TAS19AV-M25A-HZ LWIR 7.5-14 µm thermal camera. The resolution, accuracy, sensitivity and the frame rate of the camera were 640 × 480 pixels (>300,000 pixels), NEDT (noise equivalent differential temperature) < 0.03 °C and 25 frames/s, respectively.

Supplementary Materials:

Movie S1 represents evaporation of a 5µL 25.9% w/w aqueous NaCl drop placed on the superhydrophobic surface (side view) (speed 64X). The temperature of the superhydrophobic surface is t = 25°C.

Movie S2 represents evaporation of a 5µL 25.9% w/w aqueous NaCl drop placed on a superhydrophobic surface (top view) (speed 4X). The temperature of the superhydrophobic surface is t = 70°C.

Movie S3 represents evaporation of a 10 µL liquid marble made by lycopodium powder and filled with 25.9% w/w aqueous NaCl solution (side view). The temperature of the superhydrophobic surface is t = 70°C.

Acknowledgements

The authors are thankful to Mrs. Yelena Bormashenko for her kind help in preparing this manuscript.

Author Contributions

S.S. and E. B. proposed the concept. P. K. R. and I. L. designed and performed the experiments. E.B. wrote the paper. The results were analyzed by S. S., E. B., I. L. and P. K. R.

Conflict of Interest

The authors declare no conflict of interest.

References

1. Ning, N.; Fu, S.; Zhang, W.; Chen, F.; Wang, K.; Deng, H.; Zhang, Q.; Fu Q. Realizing the enhancement of interfacial interaction in semicrystalline polymer/filler composites via interfacial crystallization. *Prog. Polym. Sci.* **2012**, *37*, 1425-1455.

2. Ochoa, M.; Collazosa, N.; Lea, T.; Subramaniam, R.; Sanders, M.; Singh, R. P.; Depan, D. Nanocellulose-PE-b-PEG copolymer nanohybrid shish-kebab structure via interfacial crystallization. *Carbohydr. Polym.* **2017**, *159*, 116-124.
3. Yang, Z.; Gong, F.; He, G.; Li, Y.; Ding, L.; Nie, F.; Huan, F. Perfect Energetic Crystals with Improved Performances Obtained by Thermally Metastable Interfacial Self-Assembly of Corresponding Nanocrystals. *Cryst. Growth Des.* **2018**, *18*, 1657-1665.
4. Miyazawa, K.; Kuwasaki, Y.; Obayashi, A.; Kuwabara, K. C60 Nanowhiskers Formed by the Liquid–liquid Interfacial Precipitation Method. *J. Mater. Res*. **2002,** *17*, 83-88.
5. Tanaka, M.; Yamanaka, S.; Shirakawa, Y.; Shimosaka, A.; Hidaka, J. Preparation of porous particles by liquid–liquid interfacial crystallization. *Adv. Powder Technol*. **2011**, *22*, 125-130.
6. Kadota, K.; Shirakawa, Y.; Matsumoto, I.; Shimosaka, A.; Hidaka, J. Formation and morphology of asymmetric NaCl particles precipitated at the liquid-liquid interface. *Adv. Powder Technol.* **2007**, *18*, 775-785.
7. Tai, C.Y.; Wu, J.-F.; Rousseau, R.W. Interfacial supersaturation, secondary nucleation, and crystal growth. *J. Cryst. Growth* **1992,** *116*, 294-306.
8. Schmelzer, J.; Möller, J.; Gutzow, I.; Pascov, R.; Müller, R.; Pannhorst, W. Surface energy and structure effects on surface crystallization. *J. Non-Cryst. Solids* **1995**, *183*, 215-233.
9. Abyzov, A.S.; Schmelzer, J.W.P. Generalized Gibbs' approach in heterogeneous nucleation. *J. Chem. Phys*. **2013**, *138*, 164504.
10. Abyzov, A.S.; Davydov, L. N.; Schmelzer, J.W.P. Heterogeneous Nucleation in Solutions on Rough Solid Surfaces: Generalized Gibbs Approach. *Entropy* **2019**, *21*, 782.
11. Aussillous, P.; Quéré, D. Liquid marbles. *Nature* **2001**, *411*, 924-927.
12. Tenjimbayashi, M.; Watanabe, Y.; Nakamura, Y.; Naito, M. Exceptional Robustness and Self-Reconfigurability of Liquid Marbles on Superhydrophobic Substrate. *Adv. Mater. Interfaces* **2020**, *7*, 2000160.
13. Li, X. Liquid marbles and liquid plasticines with nanoparticle monolayers. *Adv. Colloid Interface Sci.* **2019**, *271*, 101988.
14. Bormashenko, E. Liquid Marbles, Elastic Nonstick Droplets: From Minireactors to Self-Propulsion. *Langmuir* **2017**, *33*, 663-669.
15. Arbatan, T.; Li, L.; Tian, J.; Shen, W. Liquid Marbles as Micro-bioreactors for Rapid Blood Typing. *Adv. Healthc. Mater.* **2012**, *1*, 80-83.
16. Tian, J.; Fu, N.; Chen, X. D.; Shen, W. Respirable liquid marble for the cultivation of microorganisms. *Colloids Surf. B* **2013**, *106*, 187-190.
17. Serrano, M.C.; Nardecchia, S.; Gutiérrez, M.C.; Ferrer, M.L.; del Monte, F. Mammalian Cell Cryopreservation by Using Liquid Marbles. *ACS Appl. Mater. Interfaces* **2015**, *7*, 3854-3860.
18. Vadivelu, R.K.; Ooi, Ch.H.; Yao, R.-Q.; Velasquez, J.T.; Pastrana, E.; Nido, J.D.; Lim, F.; Ekberg, J.A.K.; Nguyen, N.-Tr.; St John, J.A. Generation of three-dimensional multiple spheroid model of olfactory ensheathing cells using floating liquid marbles. *Sci. Rep.* **2015**, *5*, 1508.

19. Chen, M.; Shah, M.P.; Shelper, T.B.; Nazareth, L.; Barker, M.; Velasquez, J.T.; Ekberg, J.A.K.; Vial, M.L.; St John, J.A. Naked Liquid Marbles: A Robust Three-Dimensional Low-Volume Cell-Culturing System. *ACS Appl. Mater. Interfaces* **2019**, 11, 9814-9823.
20. Rychecký, O.; Majerská, M.; Král, V.; Štěpánek, F.; Čejková, J. Spheroid cultivation of HT-29 carcinoma cell line in liquid marbles. *Chem. Pap.* **2017**, 71, 1055-1063.
21. Sreejith, K.R.; Gorgannezhad, L.; Jin, J.; Ooi, C.H.; Stratton, H.; Dao, D.V.; Nguyen, N.-T. Liquid marbles as biochemical reactors for the polymerase chain reaction. *Lab Chip* **2019**, 19, 3220-3227.
22. Nguyen, N.K.; Ooi, C.H.; Singha, P.; Jin, J.; Sreejith, K.R.; Phan, H.P.; Nguyen, N.-T. Liquid Marbles as Miniature Reactors for Chemical and Biological Applications. *Processes* **2020**, 8, 793.
23. Dandan, M.; Erbil, H.Y. Evaporation Rate of Graphite Liquid Marbles: Comparison with Water Droplets. *Langmuir* **2009**, 25, 8362-8367.
24. Tosun, A.; Erbil, H.Y. Evaporation rate of PTFE liquid marbles. *Appl. Surf. Sci.* **2009**, 256, 1278-1283.
25. Sreejith, K.R.; Ooi, C.H.; Dao, D.V.; Nguyen, N.-T. Evaporation dynamics of liquid marbles at elevated temperatures. *RSC Adv.* **2018**, 8, 15436-15443.
26. Fullarton, C.; Draper, T.C.; Phillips, N.; Mayne, R.; de Lacy Costello, B.P.J.; Adamatzky, A. Evaporation, Lifetime, and Robustness Studies of Liquid Marbles for Collision-Based Computing. *Langmuir* **2018**, 34, 2573-2580.
27. Fullarton, C.; Draper, T.C.; Phillips, N.; de Lacy Costello, B.P.J.; Adamatzky, A. Belousov-Zhabotinsky reaction in liquid marbles. *JPhys Mater.* **2019**, *2*, 015005.
28. Adamatzky, A.; Fullarton, C.; Phillips, N.; de Lacy Costello, B.; Draper, T.C. Thermal switch of oscillation frequency in Belousov-Zhabotinsky liquid marbles. *R. Soc. Open Sci.* **2019**, *6*, 190078.
29. Draper, T.C.; Fullarton, C.; Phillips, N.; de Lacy Costello, B.P.J.; Adamatzky, A. Liquid marble interaction gate for collision-based computing. *Mater. Today* **2017**, *20*, 561-568.
30. Draper, T.C.; Phillips, N.; Weerasekera, R.; Mayne, R.; Fullarton, C.; de Lacy Costello, B.P.J.; Adamatzky, A. Contactless sensing of liquid marbles for detection, characterisation & computing. *Lab Chip* **2020**, 20, 136-146.
31. Paven, M.; Mayama, H.; Sekido, T.; Butt, H.J.; Nakamura, Y.; Fujii, S. Light-Driven Delivery and Release of Materials Using Liquid Marbles. *Adv. Funct. Mater.* **2016**, *26*, 3199-3206.
32. Fujii, S.; Yusa, S.I.; Nakamura, Y. Stimuli-Responsive Liquid Marbles: Controlling Structure, Shape, Stability, and Motion. *Adv. Funct. Mater.* **2016**, *26*, 7206-7223.
33. Bormashenko, E.; Bormashenko, Y.; Grynyov, R.; Aharoni, H.; Whyman, G.; Binks, B. P. Self-Propulsion of Liquid Marbles: Leidenfrost-like Levitation Driven by Marangoni Flow. *J. Phys. Chem. C* **2015**, *119*, 9910-9915.
34. Ooi, C.H.; Jin, J.; Nguyen, A.V.; Evans, G.M.; Nguyen, N.-T. Picking up and placing a liquid marble using dielectrophoresis. *Microfluid. Nanofluidics* **2018**, *22*, 142.

35. Jin, J.; Ooi, C.H.; Sreejith, K.R.; Dao, D.V.; Nguyen, N.-T. Dielectrophoretic Trapping of a Floating Liquid Marble. *Phys. Rev. Appl.* **2019**, *11*, 044059.
36. McBride, S.A.; Dash, S.; Varanasi, K.K. Evaporative Crystallization in Drops on Superhydrophobic and Liquid-Impregnated Surfaces. *Langmuir* **2018**, 34, 12350-12358.
37. Feng, L.; Zhang, Y.; Xi, J.; Zhu, Y.; Wang, N.; Xia, F.; Jiang, L. Petal Effect: A Superhydrophobic State with High Adhesive Force. *Langmuir* **2008**, 24, 4114-4119.
38. Bormashenko, E.; Stein, T.; Pogreb, R.; Aurbach, D. "Petal Effect" on Surfaces Based on Lycopodium: High-Stick Surfaces Demonstrating High Apparent Contact Angles. *J. Phys. Chem. C* **2009**, 113, 5568-5572.
39. Bhushan, B.; Nosonovsky, M. The rose petal effect and the modes of superhydrophobicity. *Philos. Trans. R. Soc. A* **2010**, 368, 4713-4728.
40. Bormashenko, E. Progress in understanding wetting transitions on rough surfaces. *Adv. Colloid Interface Sci.* **2015**, 222, 92-103.
41. Deegan, R.D.; Bakajin, O.; Dupont, T.F.; Huber, G.; Nagel, S.R.; Witten, T.A. Capillary flow as the cause of ring stains from dried liquid drops. *Nature* **1997**, *389*, 827-829.
42. Deegan, R.D.; Bakajin, O.; Dupont, T.F.; Huber, G.; Nagel, S.R.; Witten, T.A. Contact line deposits in an evaporating drop. *Phys. Rev. E* **2000**, *62*, 756-765.
43. Misyura, S.Y. The crystallization behavior of the aqueous solution of CaCl2 salt in a drop and a layer. *Sci. Rep.* **2020**, 10, 256.
44. Balderas-López, J.A.; Mandelis, A.; Garcia, J.A. Thermal-wave resonator cavity design and measurements of the thermal diffusivity of liquids. *Rev. Sci. Instrum.* **2000**, 71, 2933-2937.
45. Shahidzadeh-Bonn, N.; Rafa, S.; Bonn, D.; Wegdam, G. Salt Crystallization during Evaporation: Impact of Interfacial Properties. *Langmuir* **2008**, 24, 8599-8605.
46. Burton, J.C.; Sharpe, A.L.; van der Veen, R.C.A.; Franco, A.; Nagel, S.R. Geometry of the Vapor Layer Under a Leidenfrost Drop. *Phys. Rev. Lett.* **2012**, 109, 074301.

Preprints (www.preprints.org) | NOT PEER-REVIEWED | Posted: 25 September 2020 doi:10.20944/preprints202009.0616.v1

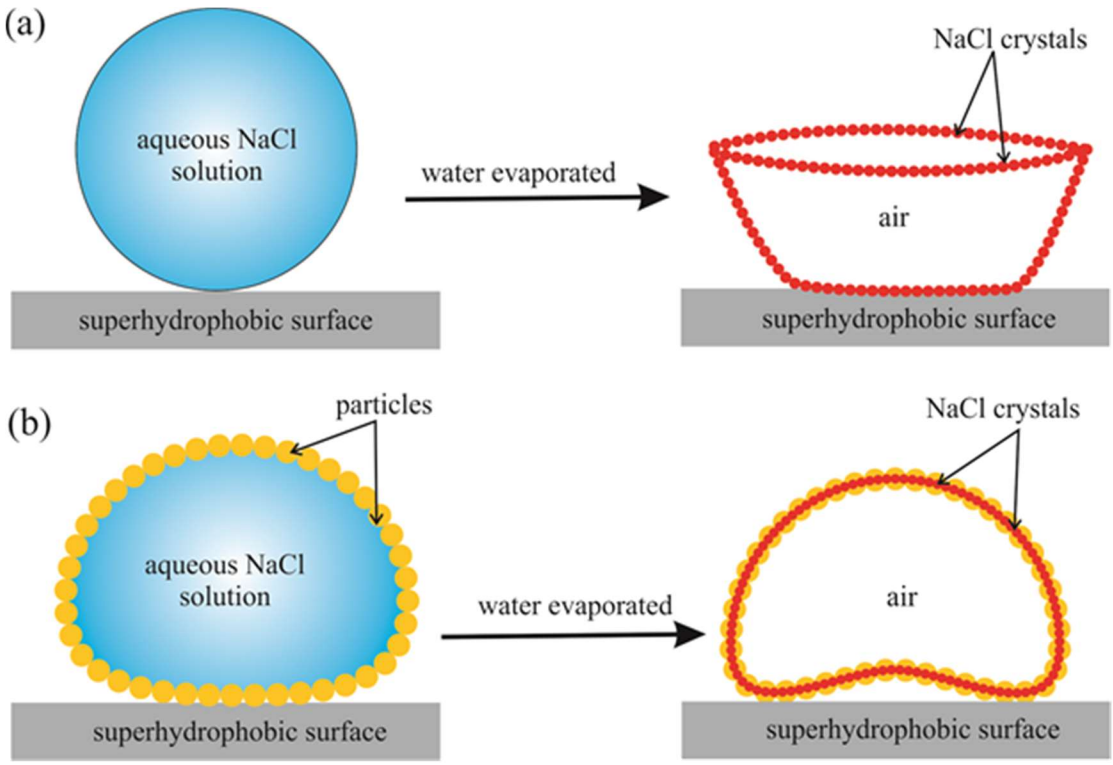

Figure 1: The evaporation processes of a naked aqueous NaCl solution drop (a) and a liquid marble filled with aqueous NaCl solution (b) placed on a superhydrophobic surface are depicted.

Preprints (www.preprints.org) | NOT PEER-REVIEWED | Posted: 25 September 2020 doi:10.20944/preprints202009.0616.v1

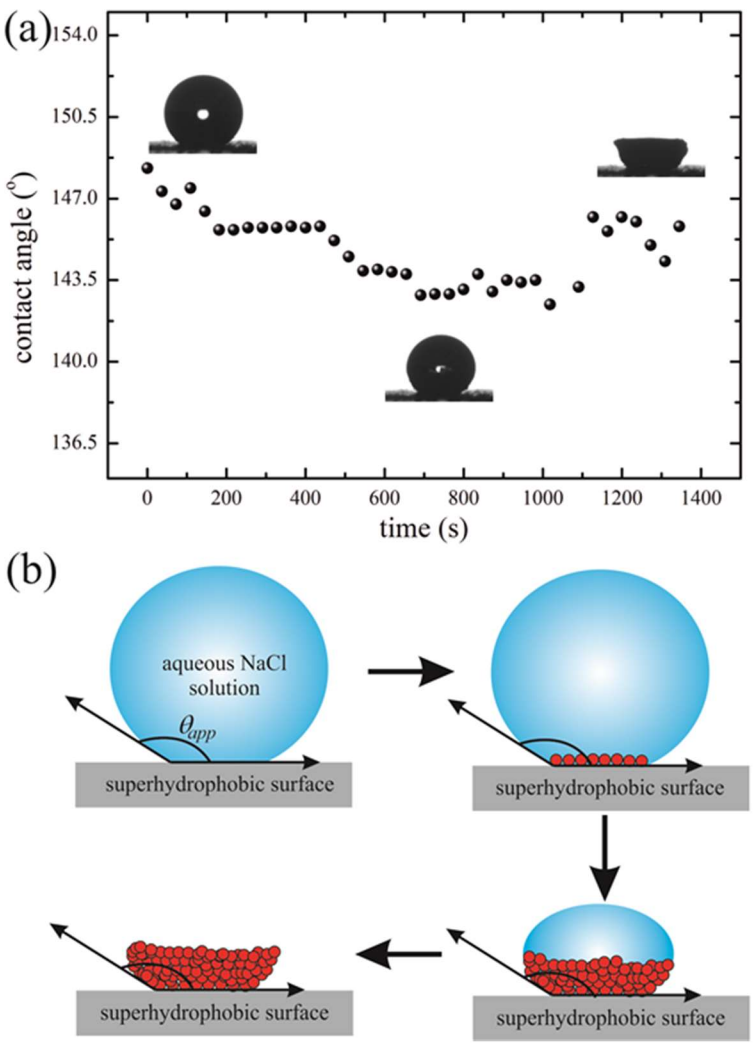

Figure 2: (a) Change in the apparent contact angle in the course of evaporation of a 5 µL 25.9% w/w aqueous NaCl drop placed on a superhydrophobic surface is shown; the temperature of evaporation t=25°C. (b) Sketch demonstrating the formation of cup-shaped residue in a course evaporation of a naked aqueous NaCl drop placed on a superhydrophobic surface is presented.

Preprints (www.preprints.org) | NOT PEER-REVIEWED | Posted: 25 September 2020 doi:10.20944/preprints202009.0616.v1

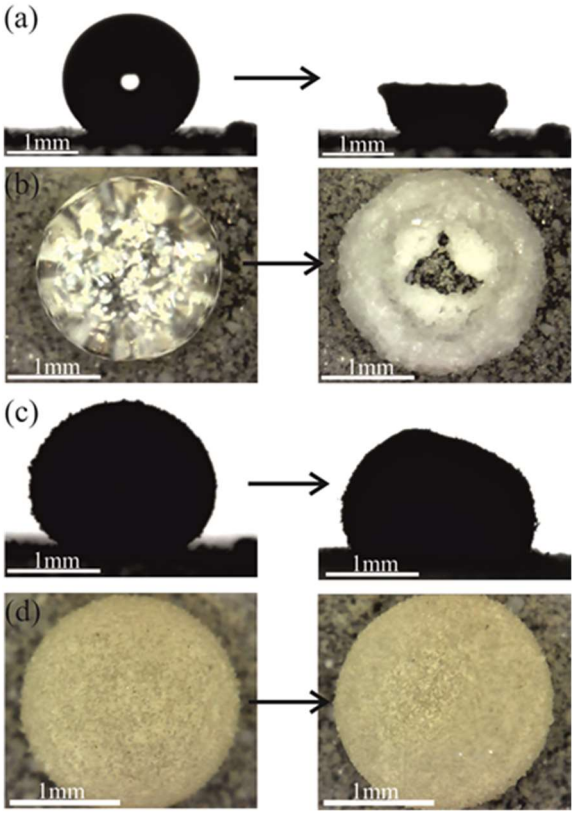

Figure 3: Comparison of evaporation of drop *vs*. liquid marble images is presented. (a), (b) represent side view and top view of 10 µL aqueous NaCl drop (c), (d) represent side view and top view of 10 µL liquid marble (liquid marbles are made by lycopodium powder and filled with 25.9% w/w aqueous NaCl solution). The temperature of superhydrophobic surface is t=70°C.

Preprints (www.preprints.org) | NOT PEER-REVIEWED | Posted: 25 September 2020 doi:10.20944/preprints202009.0616.v1

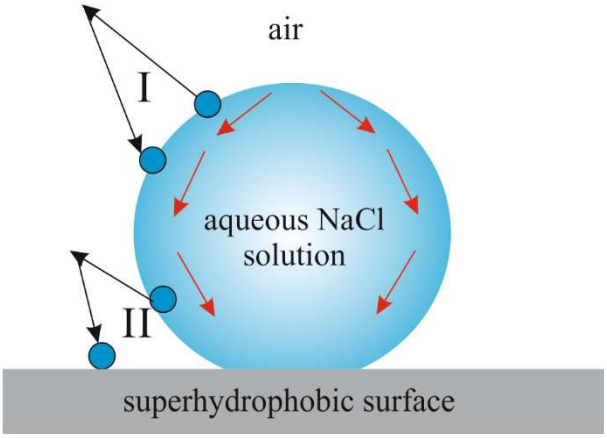

Figure 4: Scheme illustrating the formation of the coffee-stain deposits under evaporation of naked saline droplet evaporated on superhydrophobic surfaces. A molecule evaporated from the state labeled "I" has a chance to be absorbed by a droplet, whereas a molecule evaporated from site "II" has a chance to be absorbed by the superhydrophobic substrate. Red arrows illustrate the internal flows resulting in the formation of the NaCl residue.

Preprints (www.preprints.org) | NOT PEER-REVIEWED | Posted: 25 September 2020 doi:10.20944/preprints202009.0616.v1

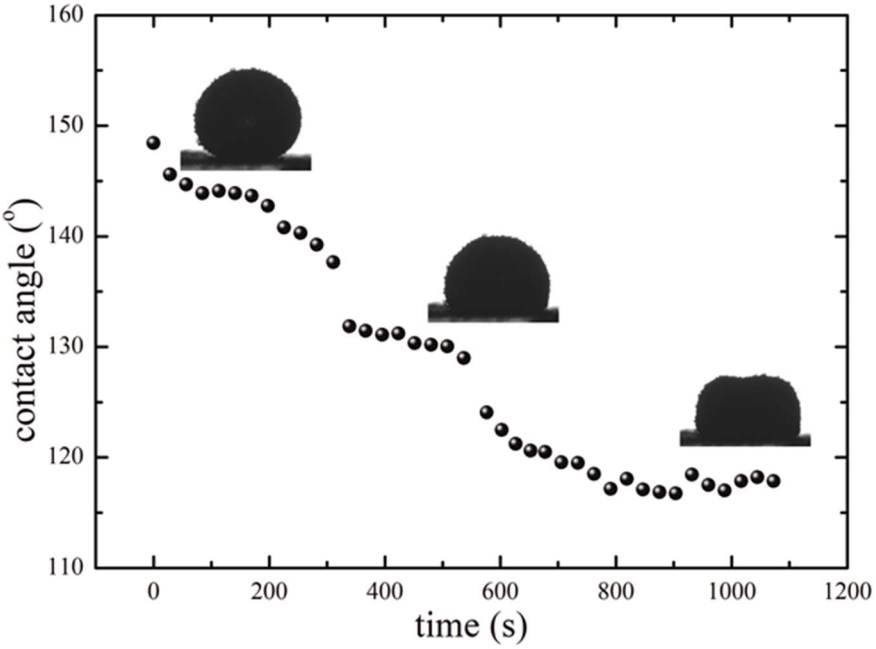

Figure 5: Change in the apparent contact angle in the course of evaporation of a 10 μL liquid marble filled with 25.9% w/w aqueous NaCl solution is presented. The temperature of the superhydrophobic surface is t=25°C.

Preprints (www.preprints.org) | NOT PEER-REVIEWED | Posted: 25 September 2020 doi:10.20944/preprints202009.0616.v1

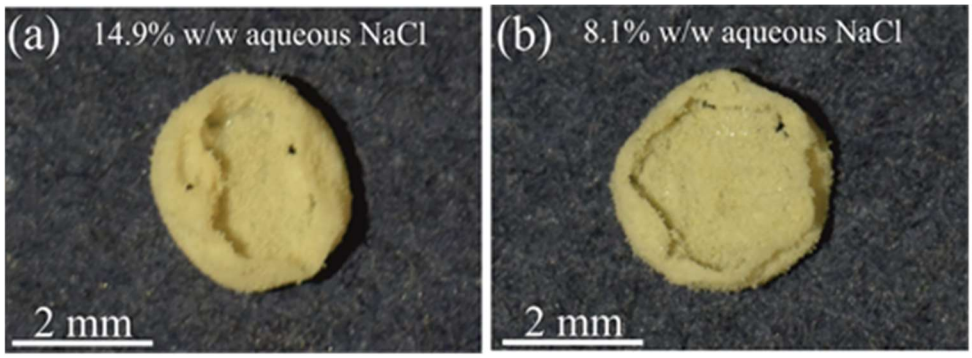

Figure 6: The photos of the residues emerging from the evaporation of 10 µL liquid marble coated by lycopodium powder and filled with 14.9% w/w (a) and 8.1% w/w (b) aqueous NaCl solution are shown. The temperature of the superhydrophobic surface is t=70°C.

Figure 7: (a) Photo of the 10 µL liquid marbles filled by 25.9% w/w NaCl solution coated by lycopodium. (b) and (c) are the photo and scanning electron microscope (SEM) images of the shell emerging from evaporation of the liquid marbles (t=70°C) respectively.

Preprints (www.preprints.org) | NOT PEER-REVIEWED | Posted: 25 September 2020 doi:10.20944/preprints202009.0616.v1

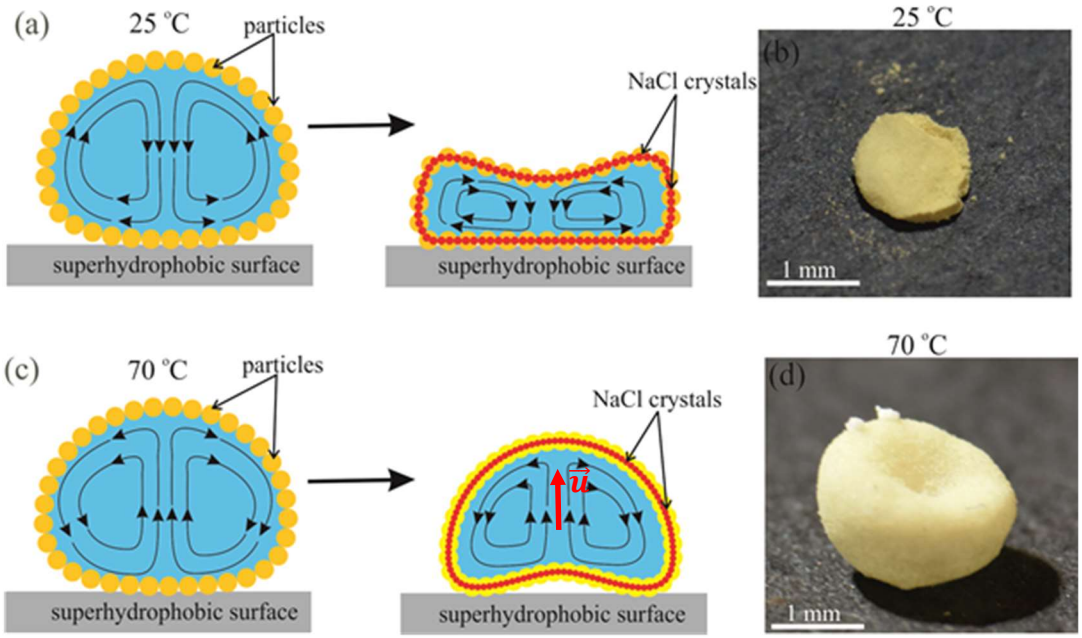

Figure 8: Water flows within marbles containing 10μL of 25.9% w/w saline and evaporated at the temperatures t=25°C and t=70°C are shown in insets (a) and (c). The shapes of the eventual NaCl deposits arising from evaporation of the marbles are shown in insets (b) and (d). The red arrow in inset (c) indicates the velocity of convective flows $\vec{u}$.

Preprints (www.preprints.org) | NOT PEER-REVIEWED | Posted: 25 September 2020 doi:10.20944/preprints202009.0616.v1

TOC image